Phys. Lett. B 880 (2026) 140846

Contents lists available at ScienceDirect

Physics Letters B

journal homepage: www.elsevier.com/locate/physletb

Letter

Semistochastic heat-bath configuration interaction with *ab initio* valence-space Hamiltonians for neutron-rich Ni, Cu, and Zn isotopes

P.Y. Wang [a,b], K.H. Li [a,c], Q. Yuan [a,d], W.J. Huang [b], J.G. Li [a,d,e,*]

[a] State Key Laboratory of Heavy Ion Science and Technology, Institute of Modern Physics, Chinese Academy of Sciences, Lanzhou, 730000, China
[b] Advanced Energy Science and Technology Guangdong Laboratory, Huizhou, 516007, China
[c] College of Physics, Center for Theoretical Physics, Henan Normal University, Xinxiang, 453007, China
[d] School of Nuclear Science and Technology, University of Chinese Academy of Sciences, Beijing, 100049, China
[e] Southern Center for Nuclear-Science Theory (SCNT), Institute of Modern Physics, Chinese Academy of Sciences, Huizhou, 516000, Guangdong Province, China

ARTICLE INFO

Editor: Baha Balantekin

Keywords:
Semistochastic heat-bath configuration interaction
Ab initio valence-space Hamiltonians
$N = 50$ shell closure
^{78}Ni

ABSTRACT

Neutron-rich nuclei around ^{78}Ni provide an important testing ground for the $N = 50$ shell closure and cross-shell correlations. We develop a nuclear-structure implementation of the semistochastic heat-bath configuration interaction (SHCI) method and apply it, for the first time, to nuclear structure calculations with *ab initio* valence-space Hamiltonians. SHCI builds a compact variational space through heat-bath selection and accounts for remaining correlations using semistochastic second-order perturbation theory. Combined with valence-space in-medium similarity renormalization group Hamiltonians derived from chiral two- and three-nucleon interactions, SHCI provides a large-space solver for extended proton-pf and neutron-gds valence spaces beyond conventional exact diagonalization. Benchmark calculations for ^{78}Ni show that SHCI achieves faster convergence of low-lying spectra than comparable particle-hole truncations, demonstrating the efficiency of determinant-based selection. We further study the $N = 50$ isotones and the Ni, Cu, and Zn isotopic chains toward the predicted neutron-rich limits. The results indicate a robust but gradually weakened $N = 50$ shell closure from Ni to Zn, predict the drip-line nuclei, and suggest a possible weak subshell structure near $N = 58$. This work establishes SHCI as a systematically improvable large-space solver for *ab initio* nuclear structure.

1. Introduction

The region around ^{78}Ni is one of the clearest laboratories for testing how traditional magic numbers evolve at the neutron-rich frontier. Spectroscopy of ^{78}Ni established a high 2_1^+ excitation energy and a strong closed-shell character, while also revealing low-lying structures associated with deformed intruder configurations [1–3]. Earlier isomer and mass measurements in neighboring Zn isotopes already pointed to a robust $N = 50$ gap near $Z = 30$ and connected this region to the *r*-process waiting point at ^{80}Zn [4–6]. Thus, nuclei around ^{78}Ni simultaneously probe shell evolution, deformation, neutron-rich limits, and astrophysical input for rapid neutron capture.

Recent experiments have provided stringent probes of shell evolution and collectivity in the neighboring Cu and Zn isotopes around ^{78}Ni [7–9]. Precision mass measurements of $^{75-79}$Cu constrain the neutron-separation-energy systematics up to $N = 50$, one proton above ^{78}Ni, and therefore provide direct information on the persistence of the shell gap [10]. In-beam γ-ray spectroscopy of ^{79}Cu and electromagnetic-moment measurements of neutron-rich Cu isotopes further support a largely persistent $Z = 28$ closure and reduced dynamical correlations toward $N = 50$ [11,12]. For neutron-rich Zn isotopes, transfer reactions and in-beam γ-ray spectroscopy of $^{79-84}$Zn have mapped single-particle strength, low-lying collective states, and intruder configurations associated with neutron particle-hole excitations across $N = 50$ [13–17]. Recent in-flight fission experiments at RIKEN have extended the known neutron-rich boundary in this region, including the identification of very neutron-rich Cu isotopes up to ^{85}Cu [18]. Together, these developments make the description of spectra, ground-state energies, separation energies, and neutron-rich limits in the Ni, Cu, and Zn region a stringent test of nuclear models.

The same region has also been investigated extensively from the theoretical side using large-scale shell model [3,19–21], Monte Carlo shell-model (MCSM) [22], beyond-mean-field [23], and *ab initio* approaches [2,24–26]. Despite differences in many-body frameworks and interactions, these studies consistently indicate that ^{78}Ni behaves as a strong, but not inert, doubly magic core. The $N = 50$ neutron gap and the $Z = 28$ proton gap remain pronounced, while neighboring nuclei are strongly affected by quadrupole correlations, proton-neutron monopole

* Corresponding author.
E-mail address: jianguo_li@impcas.ac.cn (J.G. Li).

https://doi.org/10.1016/j.physletb.2026.140846
Received 26 June 2026; Received in revised form 8 August 2026; Accepted 9 August 2026
Available online 11 August 2026
0370-2693/© 2026 The Author(s). Published by Elsevier B.V. Funded by SCOAP³. This is an open access article under the CC BY license (http://creativecommons.org/licenses/by/4.0/).

effects, and cross-shell excitations. Such correlations can lower intruder configurations and generate shape coexistence or enhanced collectivity away from ^{78}Ni [3,19–21,24]. Recent valence-space in-medium similarity renormalization group (VS-IMSRG) combined with the density matrix renormalization group (DMRG) has provided a description of the erosion of the $N = 50$ shell closure south of ^{78}Ni, highlighting multi-particle–multi-hole correlations beyond conventional truncations [25,27].

The remaining challenge is to treat the relevant many-body correlations in a large many-body space. VS-IMSRG calculations provide nonempirical valence-space Hamiltonians derived from chiral two- and three-nucleon interactions [28–33]. However, once neutron orbitals above the $N = 50$ shell closure are included explicitly, the resulting valence spaces rapidly exceed the reach of full diagonalization. This dimensional bottleneck has motivated hybrid and truncated solvers, including VS-IMSRG + DMRG and importance-truncated shell-model [25,34,35]. Here we employ the semistochastic heat-bath configuration interaction (SHCI) method as a complementary large-space solver for nuclear structure. SHCI selects the most important Slater determinants with a heat-bath criterion and accounts for the remaining correlation energy through a semistochastic perturbative correction [36–39]. Compared with DMRG, SHCI does not rely on orbital ordering or matrix-product-state compression, and it provides a direct determinant-selection criterion together with a perturbative correction and extrapolation scheme.

In this work, we develop a nuclear-structure implementation of the SHCI as a large-space solver and combine it with VS-IMSRG effective Hamiltonians. We first apply this framework to the spectroscopy of ^{78}Ni, where the low-lying spectrum directly probes its doubly magic character. We then extend the calculations to neighboring $N = 50$ isotones from Fe to Zn, to quantify the evolution of the $N = 50$ shell closure. Finally, we investigate the neutron-rich limits of Ni, Cu, and Zn isotopic chains. The predicted ground-state energies, two-neutron separation energies, and drip-line locations provide a unified description of shell evolution from ^{78}Ni toward the neutron drip line.

2. Theoretical framework

2.1. VS-IMSRG Hamiltonians

We start from chiral effective field theory nuclear interactions and, in the present calculations, employ the EM1.8/2.0 interaction [40–42]. Valence-space Hamiltonians are constructed using the VS-IMSRG [28,29,31–33]. The Hamiltonian is normal ordered with respect to an ensemble reference state,

$$H = E_0 + \sum_{ij} f_{ij}\{a_i^\dagger a_j\} + \frac{1}{4}\sum_{ijkl}\Gamma_{ijkl}\{a_i^\dagger a_j^\dagger a_l a_k\} + \dots, \tag{1}$$

where E_0, f, and Γ are the zero-, one-, and two-body terms. The IMSRG evolution decouples the chosen core and valence space from excluded configurations, and the Magnus formulation is used to obtain the evolved Hamiltonian and consistently transformed operators [30]. The valence space contains proton pf orbitals and neutron orbitals spanning the $N = 50$ shell closure, including the relevant gds degrees of freedom. The VS-IMSRG effective Hamiltonians are derived using the IMSRG++ code [43]. The two- and three-nucleon matrix elements of the chiral EM1.8/2.0 interaction are generated with the `NuHamil` code [44]. The nuclear interaction is calculated using $N_{\max} = 14$, $E_{3\max} = 24$, and $\hbar\omega = 16$ MeV.

2.2. Semistochastic heat-bath configuration interaction as a nuclear many-body solver

Originally developed in quantum chemistry, SHCI is employed here as a selected-CI solver for VS-IMSRG valence-space Hamiltonians in nuclear spaces beyond full diagonalization [36–39]. It provides a complementary route to large-scale shell-model calculations by constructing a compact variational space from the Slater determinants that contribute most strongly to the target states.

The variational wave function in SHCI is written as $|\Psi_{\rm var}\rangle = \sum_{D_i\in\mathcal{V}} c_i|D_i\rangle$, where $\mathcal{V}$ denotes the selected determinant space. Starting from an initial trial space, new determinants are iteratively added according to the heat-bath criterion

$$|H_{ai}c_i| > \epsilon_1, \tag{2}$$

where $D_i \in \mathcal{V}$, $D_a \notin \mathcal{V}$, and ϵ_1 controls the size of the variational space. Eq. (2) is an existence condition and does not imply a summation over the $D_i \in \mathcal{V}$. The new determinant D_a is retained if it has a sufficiently large coupling to at least one determinant in the current variational space. This differs from the importance measures based on the first-order wave-function correction, such as the IT-NCSM [35,45–48] method, which involve the coherent sum $\sum_i H_{ai}c_i$ together with an energy denominator and therefore require the evaluation of matrix-vector products. The absence of this summation makes the heat-bath criterion particularly efficient: for each variational determinant D_i, only those connected determinants satisfying $|H_{ai}| \geq \epsilon_1/|c_i|$ need to be generated. The many connected determinants that cannot satisfy the threshold are therefore never explicitly examined. The iterative selection procedure is continued until the number of newly added determinants falls below 0.1 % of the dimension of the current variational space. The resulting Hamiltonian is diagonalized only in the selected subspace, yielding variational energies and wave functions for the targeted low-lying states.

The residual correlation energy from determinants outside $\mathcal{V}$ is estimated by a second-order Epstein–Nesbet perturbative correction (PT2),

$$\Delta E_{\rm PT2} = \sum_{D_a\notin\mathcal{V}} \frac{\left|\sum_{D_i\in\mathcal{V}} H_{ai}c_i\right|^2}{E_{\rm var} - H_{aa}}. \tag{3}$$

To overcome the storage bottleneck of Eq. (3), which requires a sum over all external determinants connected to the selected space $\mathcal{V}$, SHCI introduces the second threshold $\epsilon_2 < \epsilon_1$ in the perturbative step, where the restricted sum includes only terms satisfying $|H_{ai}c_i| \geq \epsilon_2$. Large PT2 contributions are evaluated deterministically, while the remaining small contributions can be included semistochastically [36–39]. At a finite selection threshold, the SHCI energy is $E_{\rm SHCI} = E_{\rm var} + \Delta E_{\rm PT2}$. Calculations are repeated for a sequence of decreasing ϵ_1 values, producing a set of variational energies and PT2 corrections. The selected-space limit is obtained by extrapolating $E_{\rm SHCI}$ as a function of $|\Delta E_{\rm PT2}|$ to $|\Delta E_{\rm PT2}| = 0$ [38]. Linear extrapolations are used as the default, and the selected-space extrapolation uncertainty is estimated by varying the fit window.

As a validation, we first benchmark the SHCI in ^{71}Ni using the valence space Hamiltonian. Using $\epsilon_1 = 2\times10^{-4}$, 1×10^{-4}, 9×10^{-5}, 8×10^{-5}, and 7×10^{-5}, with $\epsilon_2 = 1\times10^{-10}$, the zero-PT2 extrapolated energy is -164.098985 ± 0.000028 MeV, which differs from the exact value of -164.098659 MeV by 0.33 keV. We further examine the sensitivity to the ϵ_1 sequence using ^{79}Cu. The above sequence gives -216.674865 ± 0.000834 MeV, while an alternative sequence, $\epsilon_1 = 2\times10^{-4}$, 1.6×10^{-4}, 1.3×10^{-4}, 1×10^{-4}, and 9×10^{-5}, gives -216.675453 ± 0.001006 MeV. The difference is only about 0.5 keV, showing that the extrapolation is insensitive to the adopted ϵ_1 sequence and that the residual external-space contribution is sufficiently small for a stable zero-PT2 extrapolation. For all remaining calculations, we use the first ϵ_1 sequence for isotopes with $N \leq 52$ and the alternative one for $N > 52$, with ϵ_2 fixed at 1×10^{-10} throughout.

Beyond providing converged energies, the dominant determinants, particle-hole content, and orbital occupations can be extracted from the same calculation, making it possible to connect the evolution of ground-state energies and spectra with the underlying shell structure and many-body correlations. Thus, the VS-IMSRG + SHCI combines *ab initio* effective Hamiltonians with a systematically improvable large-space solver and provides quantitative spectroscopic information and microscopic wave-function diagnostics for exotic nuclei.

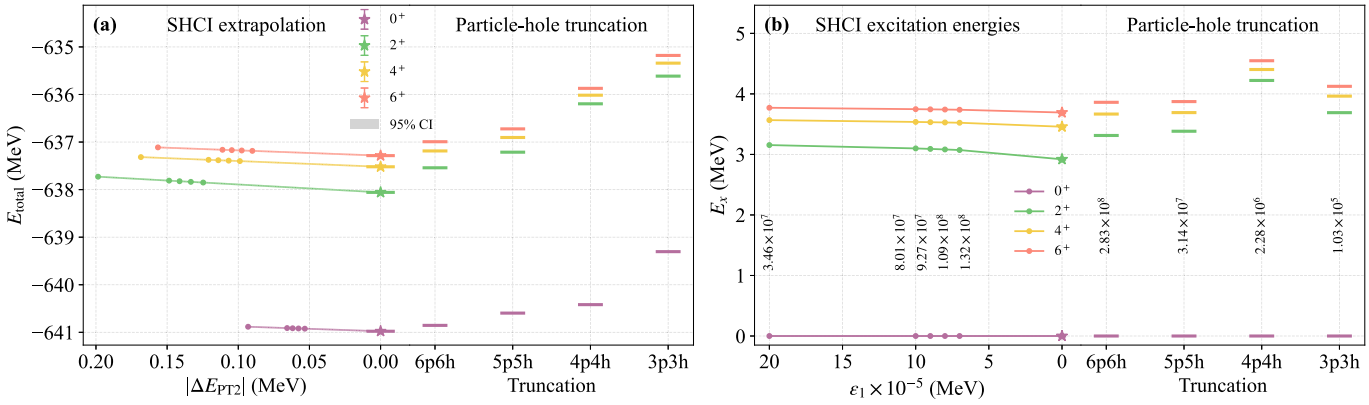


Fig. 1. Total and excitation energies of low-lying states of ^{78}Ni from SHCI and particle-hole truncated shell-model calculations. The extrapolation error of the SHCI is very small and is not clearly represented in the figure. The dimension of the full configuration-interaction model space is 2.10×10^{11}. The numbers shown in panel (b) denote the dimensions of selected SHCI and the corresponding particle-hole truncated spaces. The values at $\epsilon_1 = 0$ in panel (b) are obtained by subtracting the extrapolated energies of low-lying states in panel (a).

3. Results and discussion

3.1. SHCI convergence and spectroscopy of ^{78}Ni

We now apply the VS-IMSRG + SHCI framework introduced above to neutron-rich nuclei around ^{78}Ni. Its low-lying spectrum tests whether the selected SHCI space captures the dominant closed-shell configuration and the leading cross-shell correlations. For comparison, we also perform shell model calculations with explicit *mpmh* truncations across the $Z = 28$ and $N = 50$ shells, where $m = 3$–6 is the maximum number of particles excited across the shell closures. Fig. 1 summarizes the convergence of the lowest four states of ^{78}Ni from SHCI and compares them with the truncated shell-model results.

Fig. 1(a) shows the SHCI total energies as functions of $|\Delta E_{PT2}|$, together with the zero-PT2 extrapolations and truncated shell-model results. As ϵ_1 is lowered, the selected space grows while $|\Delta E_{PT2}|$ decreases, showing the systematic recovery of correlations outside the variational space. The nearly linear behavior of the final SHCI points supports the zero-PT2 extrapolation, with uncertainties of only several keV from different fitting windows and fit errors. The convergence is state dependent: the ground state has the smallest $|\Delta E_{PT2}|$ and converges fastest, consistent with its closed-shell character, whereas the excited states have larger PT2 corrections and are more sensitive to cross-shell correlations. A similar trend appears in the *mpmh* calculations, where the ground-state energy converges faster than the excitation spectrum, indicating stronger correlations in the low-lying excited states.

The excitation energies relative to the ground state are displayed in Fig. 1(b). For each finite selection threshold ϵ_1, the excitation energies shown in Fig. 1(b) are calculated directly as $E_x^J(\epsilon_1) = E_{total}^J(\epsilon_1) - E_{total}^{0^+}(\epsilon_1)$. Each point in Fig. 1(b) corresponds to the total-energy results obtained at the same value of ϵ_1 in Fig. 1(a), so that there is no extrapolation of the excitation energies with respect to ϵ_1. The values shown at $\epsilon_1 = 0$ are obtained from the differences between the independently extrapolated total energies in Fig. 1(a). They converge more smoothly than the absolute energies due to the partial cancellation of residual correlations. The SHCI spectrum shows the characteristic pattern of a doubly magic nucleus, with the 2_1^+ state around 3 MeV. As ϵ_1 decreases, $E_x(2_1^+)$ moves toward the experimental value of approximately 2.7 MeV [1]. The zero-PT2 extrapolation gives $E_x(2_1^+) \approx 2.93$ MeV, preserving the characteristic high-lying 2_1^+ state of a doubly magic nucleus. The particle-hole truncated spectra approach the SHCI results as the truncation is enlarged, but more slowly: even in the 6*p*6*h* space, which is slightly larger than the selected SHCI space at $\epsilon_1 = 7 \times 10^{-5}$, $E_x(2_1^+)$ remains about 200 keV above the finite-ϵ_1 SHCI value and about 400 keV above the SHCI extrapolation. This demonstrates that low-lying spectra are governed not only by the total many-body dimension, but also by the efficient selection of relevant cross-shell configurations. In SHCI, such configurations are selected variationally through the heat-bath criterion, and the residual correlation energy is incorporated through the PT2 extrapolation, leading to faster convergence.

3.2. Spectroscopy of $N = 50$ isotones

We next investigate the low-lying spectroscopy of the $N = 50$ isotones ^{80}Zn, ^{79}Cu, ^{78}Ni, ^{77}Co, and ^{76}Fe, to examine the proton-number dependence of the $N = 50$ shell closure across $Z = 28$. For each nucleus, the lowest four states are calculated using the VS-IMSRG + SHCI framework and compared with the available experimental data [1,11,49], as shown in Fig. 2. We also analyze neutron occupations relative to the naive $N = 50$ filling, where positive values above the gap and corresponding depletion below the gap quantify neutron particle-hole excitations across $N = 50$. This isotonic chain therefore probes the robustness of the $N = 50$ gap from the proton-particle side above Ni to the proton-hole side below $Z = 28$.

For the even-even isotones, the most striking feature is the much lower 2_1^+ energy in ^{76}Fe than in ^{80}Zn and ^{78}Ni. This asymmetry indicates a pronounced weakening of the $N = 50$ shell closure below ^{78}Ni, where proton holes below $Z = 28$ enhance quadrupole correlations and promote neutron particle-hole excitations across the shell gap. This behavior is consistent with previous shell-model and *ab initio* studies showing that ^{78}Ni is strongly, but not inertly, doubly magic and that *mpmh* configurations become increasingly important toward the proton-hole side [3,21,24,27]. The occupations support this interpretation: in ^{76}Fe, the sizable population of neutron orbitals above $N = 50$, especially the ds and $g_{7/2}$ orbitals, signals strong cross-shell mixing and substantial erosion of the $N = 50$ closure.

In contrast, ^{80}Zn, with two protons above the $Z = 28$ shell closure, still retains a relatively high $E(2_1^+)$, supporting the persistence of a sizable $N = 50$ shell gap on the proton-particle side of ^{78}Ni. The calculated 2_1^+ energy is about 500 keV above experiment, giving a slight overestimate of the $N = 50$ shell stiffness in ^{80}Zn. The calculated 2_1^+ energy of ^{82}Zn is 0.770 MeV, lower than that of ^{80}Zn, indicating enhanced collectivity once neutrons are added above $N = 50$. This behavior suggests that the $N = 50$ gap remains visible at $Z = 30$, but the closed-shell rigidity is softened beyond the shell closure. Consistently, the occupation analysis shows stronger neutron cross-shell excitations in ^{80}Zn than in ^{78}Ni, indicating that two protons outside the $Z = 28$ core already enhance quadrupole correlations and slightly weaken the ideal closed-shell picture. However, these cross-shell excitations remain much weaker than those in ^{76}Fe. This conclusion is consistent with

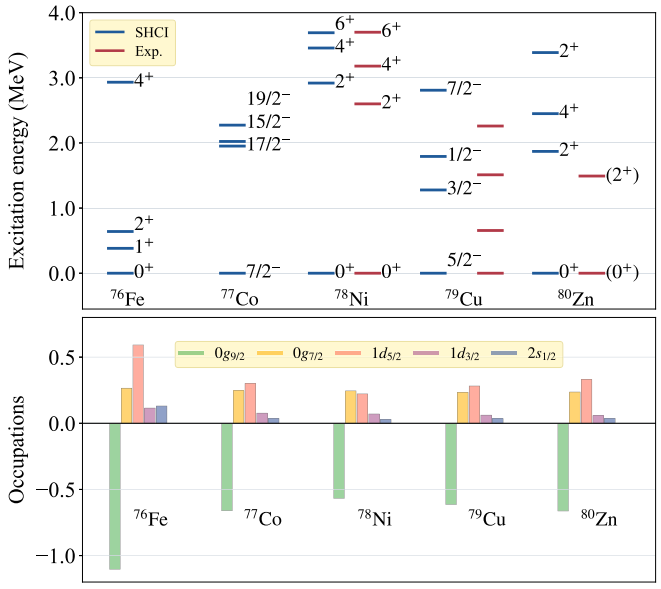


Fig. 2. Low-lying spectra and neutron occupations for the $N = 50$ isotones ^{80}Zn, ^{79}Cu, ^{78}Ni, ^{77}Co, and ^{76}Fe, calculated with VS-IMSRG + SHCI and compared with available experimental data [1,11,49]. Negative values indicate depletion below the $N = 50$ closure, while positive values indicate occupation above the closure.

experimental studies of neutron-rich Zn isotopes and mass measurements around $N = 50$, which point to a robust but gradually evolving shell closure from ^{78}Ni to ^{82}Ge [5,14–16,50]. For the odd-Z isotones ^{79}Cu and ^{77}Co, the low-lying spectra provide a complementary probe of proton-particle and proton-hole structures around the ^{78}Ni core [10–12]. The calculated level ordering in ^{79}Cu also agrees with the MCSM calculations [11].

The selected SHCI dimensions further reflect the different correlation strengths in ^{76}Fe and ^{78}Ni. At $\epsilon_1 = 7 \times 10^{-5}$, the selected space for ^{76}Fe reaches about 2.1×10^8 Slater determinants, larger than that for ^{78}Ni with 1.31×10^8 Slater determinants, despite the larger full many-body dimension of ^{78}Ni. This indicates a more fragmented wave function in ^{76}Fe. While ^{78}Ni is dominated by near-spherical closed-shell configurations, proton holes below $Z = 28$ in ^{76}Fe enhance quadrupole correlations and neutron particle-hole excitations across $N = 50$. Consequently, more determinants are required to describe its deformed and strongly mixed low-lying states, signaling a stronger erosion of the closed-shell structure.

3.3. Neutron-rich limits and shell evolution

Having established from the $N = 50$ isotones that the shell closure evolves with proton number, we now examine its consequences along the Ni, Cu, and Zn isotopic chains. The mass systematics provide a complementary probe of the same physics: ground-state energies determine the neutron-rich limits, while separation energies and empirical shell gaps quantify the persistence and softening of the shell closure away from ^{78}Ni. Fig. 3 shows the ground-state energies, two-neutron separation energies (S_{2n}), and empirical two-neutron shell gaps for neutron-rich Ni, Cu, and Zn isotopes. The calculated VS-IMSRG + SHCI results are compared with available experimental and extrapolated masses from AME2020 [51].

Fig. 3(a) shows that the calculated ground-state energies follow the experimental systematics from Ni to Zn. The remaining deviations vary smoothly along each isotopic chain, suggesting that the relative trends are more robust than the absolute ground-state energies. We use these ground-state energies to determine the neutron-rich limits. The one- and two-neutron drip lines are identified separately. The last isotope

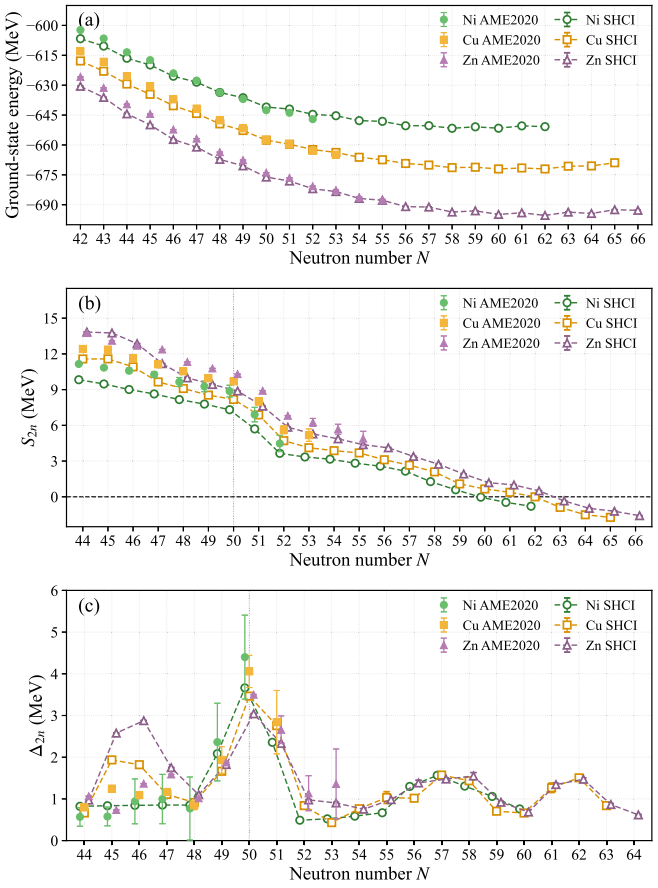


Fig. 3. Ground-state energies, two-neutron separation energies, and empirical two-neutron shell gaps of Ni, Cu, and Zn isotopes calculated with VS-IMSRG + SHCI up to the predicted neutron drip lines. The error bars of the SHCI results indicate the extrapolation uncertainties; unless otherwise visible, they are smaller than the corresponding plotting symbols. The results are compared with available experimental and extrapolated masses from AME2020 [51], and used to identify the neutron-rich limits and the evolution of the $N = 50$ shell closure.

with positive S_n defines the one-neutron drip line, while the last isotope with positive S_{2n} defines the two-neutron drip line. Although only S_{2n} is shown in Fig. 3, the one-neutron separation energies are calculated from the same ground-state energies and are used to identify the one-neutron drip lines. Within the present Hamiltonian and valence-space truncation, the predicted drip-line nuclei from the one-neutron criterion are ^{83}Ni, ^{86}Cu, and ^{87}Zn. For the two-neutron criterion, the predicted last bound nuclei are ^{86}Ni, ^{91}Cu, and ^{92}Zn.

Experimentally, the neutron-rich frontier in the Ni, Cu, and Zn region has been steadily extended at RIKEN. The most neutron-rich isotopes observed so far include ^{81,82}Ni, ^{85}Cu, and ^{84,85}Zn, while recent precision mass measurements have reached neutron-rich Zn isotopes such as ^{83}Zn [7,18,52,53]. These limits remain well inside the region covered by the present VS-IMSRG + SHCI calculations. Global mass models, such as Skyrme-HFB and FRDM(2012), also place the Ni, Cu, and Zn drip lines far beyond the known isotopes, although the detailed locations differ among models [54–56]. The present results provide a complementary *ab initio* prediction based on chiral interactions and a systematically improvable selected-CI solver. Near the drip line, however, the small separation energies make the exact locations sensitive to residual uncertainties from the VS-IMSRG Hamiltonian, SHCI calculation, and omitted continuum coupling.

We now turn to the shell evolution encoded in the same mass systematics. Fig. 3(b) shows the S_{2n}, which measures the additional

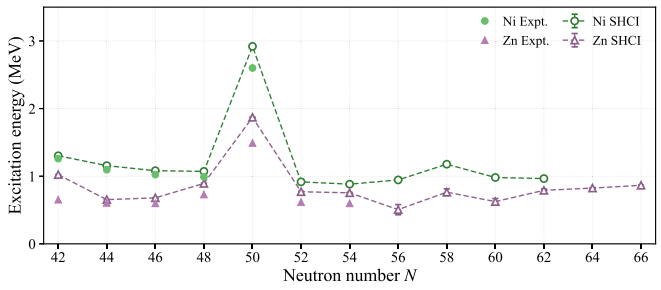


Fig. 4. First 2^+ excitation energies of even-even Ni and Zn isotopes calculated with VS-IMSRG + SHCI and compared with available experimental data [49].

binding gained by adding two neutrons. In all three isotopic chains, S_{2n} decreases with increasing neutron number, with a visible change of slope across $N = 50$. This behavior reflects the persistence of the neutron shell closure around ^{78}Ni. The effect is most pronounced in the Ni chain, where the drop of S_{2n} beyond $N = 50$ is steeper. For Cu and Zn, the decrease beyond $N = 50$ is smoother, indicating that valence protons outside the $Z = 28$ core enhance proton-neutron correlations and reduce the rigidity of the $N = 50$ shell closure.

To quantify this shell effect, we consider the empirical two-neutron shell gap, $\Delta_{2n}(Z, N) = S_{2n}(Z, N) - S_{2n}(Z, N + 2)$. As shown in Fig. 3(c), Δ_{2n} exhibits a clear peak at $N = 50$ for Ni, Cu, and Zn. The largest peak appears in the Ni chain, consistent with a robust $N = 50$ shell closure at ^{78}Ni. Moving from Ni to Cu and Zn, the peak at $N = 50$ is reduced, showing that the shell gap is gradually weakened by the addition of one or two protons outside the $Z = 28$ core. The results are in agreement with the occupation analysis presented above. Away from $N = 50$, Δ_{2n} is smaller and varies more smoothly, indicating that the enhanced stability is localized around the shell closure rather than being a smooth bulk effect. The combined S_{2n} and Δ_{2n} systematics therefore show that the $N = 50$ shell closure remains strongest at $Z = 28$, but becomes progressively softened toward Cu and Zn as proton-neutron correlations and neutron cross-shell excitations increase.

The shell evolution inferred from masses is further tested by the first 2^+ excitation energies of even-even Ni and Zn isotopes, shown in Fig. 4. The $E_x(2_1^+)$ is a sensitive spectroscopic indicator of the competition between shell closure and quadrupole collectivity: a high $E_x(2_1^+)$ is characteristic of a closed-shell configuration, whereas a rapid decrease signals enhanced correlations and deformation. In the Ni chain, the calculated $E_x(2_1^+)$ exhibits a pronounced maximum at $N = 50$, consistent with the doubly magic character of ^{78}Ni. Away from $N = 50$, the $E_x(2_1^+)$ decreases, indicating the onset of collectivity as the closed-shell configuration is broken.

A similar but softened pattern is found in the Zn chain. The calculated 2_1^+ energy also increases around $N = 50$, showing that the neutron shell gap remains visible when two protons are added outside the $Z = 28$ core. However, the peak is lower than in Ni and the decrease beyond $N = 50$ is more gradual. This is consistent with the S_{2n} and Δ_{2n} trends: the $N = 50$ shell closure persists in Zn, but proton-neutron correlations and neutron particle-hole excitations across the gap reduce the rigidity of the closed-shell structure. Beyond the dominant $N = 50$ closure, Δ_{2n} shows weak local enhancements near $N = 58$ and $N = 62$. These features are much smaller than the $N = 50$ peak. The 2_1^+ systematics provide partial support only for the $N = 58$ feature, where a mild increase of $E_x(2_1^+)$ is found, whereas no corresponding enhancement appears near $N = 62$. This suggests a possible weak subshell structure around $N = 58$, which should be tested by future mass and spectroscopy measurements.

Overall, Figs. 3 and 4 connect the predicted neutron-rich limits with shell evolution around ^{78}Ni. The ground-state and separation energies determine how far the Ni, Cu, and Zn chains remain bound, while Δ_{2n} and the 2_1^+ energies quantify the persistence and gradual softening of the $N = 50$ shell closure. In this context, the SHCI method provides a crucial computational tool that makes such large-scale valence-space calculations feasible, extending well beyond conventional shell-model diagonalization capabilities.

4. Summary

We have developed a nuclear-structure implementation of the semistochastic heat-bath configuration interaction method and applied it for the first time to nuclear structure calculations with *ab initio* valence-space Hamiltonians. Important Slater determinants are selected through a heat-bath criterion, while remaining correlations are treated by semistochastic second-order perturbation theory and zero-PT2 extrapolation. Combined with VS-IMSRG Hamiltonians, SHCI provides a systematically improvable solver for large valence spaces beyond conventional exact diagonalization.

As a benchmark, we studied ^{78}Ni with VS-IMSRG + SHCI. SHCI yields stable low-lying energies with uncertainties of only several keV and converges faster than comparable particle-hole truncation schemes, highlighting its ability to efficiently capture the most important cross-shell configurations. We then investigated the $N = 50$ isotones from ^{76}Fe to ^{80}Zn. The results show that the $N = 50$ shell closure is strongest near ^{78}Ni but evolves with proton number. Proton holes below $Z = 28$ enhance quadrupole correlations and neutron excitations, significantly weakening the closure in ^{76}Fe, whereas ^{80}Zn retains a visible shell gap despite signs of gradual softening. Finally, we extended the Ni, Cu, and Zn isotopic chains toward the neutron drip line. The last bound nuclei are predicted to be ^{83}Ni, ^{86}Cu, and ^{87}Zn from S_n, and ^{86}Ni, ^{91}Cu, and ^{92}Zn from S_{2n}. Systematics of S_{2n}, Δ_{2n}, and 2_1^+ excitation energies indicate a robust $N = 50$ shell closure at $Z = 28$ that gradually weakens toward Zn, while weak signatures around $N = 58$ suggest a possible subshell structure.

This work establishes SHCI as a powerful, systematically improvable selected-CI solver for large-scale nuclear structure calculations, demonstrating its capability for *ab initio* calculations combined with valence-space Hamiltonians.

Declaration of competing interest

The authors declare that they have no known competing financial interests or personal relationships that could have appeared to influence the work reported in this paper.

Acknowledgements

This work has been supported by the National Key R&D Program of China under Grant Nos. 2024YFE0109800, 2024YFE0109802, and 2023YFA1606403; The National Natural Science Foundation of China under Grant Nos. 12405141, 12347106, 12441506, 12575124, 12375123. The numerical calculations in this paper have been done at Hefei Advanced Computing Center.

Data availability

Data will be made available on request.

References

[1] R. Taniuchi, C. Santamaria, P. Doornenbal, A. Obertelli, K. Yoneda, G. Authelet, H. Baba, D. Calvet, F. Château, A. Corsi, A. Delbart, J.-M. Gheller, A. Gillibert, J.D. Holt, T. Isobe, V. Lapoux, M. Matsushita, J. Menéndez, S. Momiyama, T. Motobayashi, M. Niikura, F. Nowacki, K. Ogata, H. Otsu, T. Otsuka, C. Péron, S. Péru, A. Peyaud, E.C. Pollacco, A. Poves, J.-Y. Roussé, H. Sakurai, A. Schwenk, Y. Shiga, J. Simonis, S.R. Stroberg, S. Takeuchi, Y. Tsunoda, T. Uesaka, H. Wang, F. Browne, L.X. Chung, Z. Dombradi, S. Franchoo, F. Giacoppo, A. Gottardo, K. Hadyńska-Klęk, Z. Korkulu, S. Koyama, Y. Kubota, J. Lee, M. Lettmann, C. Louchart, R. Lozeva, K. Matsui, T. Miyazaki, S. Nishimura, L. Olivier, S. Ota, Z. Patel, E. Şahin, C. Shand, P.-A. Söderström, I. Stefan, D. Steppenbeck, T. Sumikama, D. Suzuki, Z. Vajta, V. Werner, J. Wu, Z.Y. Xu, ^{78}Ni revealed as a doubly magic stronghold against nuclear deformation, Nature 569 (7754) (2019) 53–58. https://doi.org/10.1038/s41586-019-1155-x

[2] G. Hagen, G.R. Jansen, T. Papenbrock, Structure of ^{78}Ni from first-principles computations, Phys. Rev. Lett. 117 (2016) 172501. https://doi.org/10.1103/PhysRevLett.117.172501

[3] F. Nowacki, A. Poves, E. Caurier, B. Bounthong, Shape coexistence in ^{78}Ni as the portal to the fifth island of inversion, Phys. Rev. Lett. 117 (2016) 272501. https://doi.org/10.1103/PhysRevLett.117.272501

[4] J.M. Daugas, R. Grzywacz, M. Lewitowicz, L. Achouri, J.C. Angélique, D. Baiborodin, K. Bennaceur, R. Bentida, R. Béraud, C. Borcea, C. Bingham, W.N. Catford, A. Emsallem, G. de France, H. Grawe, K.L. Jones, R.C. Lemmon, M.J. Lopez Jimenez, F. Nowacki, F. de Oliveira Santos, M. Pfützner, P.H. Regan, K. Rykaczewski, J.E. Sauvestre, M. Sawicka, G. Sletten, M. Stanoiu, The 8^+ isomer in ^{78}Zn and the doubly magic character of ^{78}Ni, Phys. Lett. B 476 (3) (2000) 213–218. https://doi.org/10.1016/S0370-2693(00)00177-5

[5] J. Hakala, S. Rahaman, V.-V. Elomaa, T. Eronen, U. Hager, A. Jokinen, A. Kankainen, I.D. Moore, H. Penttilä, S. Rinta-Antila, J. Rissanen, A. Saastamoinen, T. Sonoda, C. Weber, J. Äystö, Evolution of the $N = 50$ shell gap energy towards ^{78}Ni, Phys. Rev. Lett. 101 (2008) 052502. https://doi.org/10.1103/PhysRevLett.101.052502

[6] S. Baruah, G. Audi, K. Blaum, M. Dworschak, S. George, C. Guénaut, U. Hager, F. Herfurth, A. Herlert, A. Kellerbauer, H.-J. Kluge, D. Lunney, H. Schatz, L. Schweikhard, C. Yazidjian, Mass measurements beyond the major *r*-process waiting point ^{80}Zn, Phys. Rev. Lett. 101 (2008) 262501. https://doi.org/10.1103/PhysRevLett.101.262501

[7] T. Sumikama, S. Nishimura, H. Baba, F. Browne, P. Doornenbal, N. Fukuda, S. Franchoo, G. Gey, N. Inabe, T. Isobe, P.R. John, H.S. Jung, D. Kameda, T. Kubo, Z. Li, G. Lorusso, I. Matea, K. Matsui, P. Morfouace, D. Mengoni, D.R. Napoli, M. Niikura, H. Nishibata, A. Odahara, E. Sahin, H. Sakurai, P.-A. Söderström, G.I. Stefan, D. Suzuki, H. Suzuki, H. Takeda, R. Taniuchi, J. Taprogge, Z. Vajta, H. Watanabe, V. Werner, J. Wu, Z.Y. Xu, A. Yagi, K. Yoshinaga, Observation of new neutron-rich Mn, Fe, Co, Ni, and Cu isotopes in the vicinity of ^{78}Ni, Phys. Rev. C 95 (2017) 051601(R). https://doi.org/10.1103/PhysRevC.95.051601

[8] C. Delafosse, D. Verney, P. Marević, A. Gottardo, C. Michelagnoli, A. Lemasson, A. Goasduff, J. Ljungvall, E. Clément, A. Korichi, G. De Angelis, C. Andreoiu, M. Babo, A. Boso, F. Didierjean, J. Dudouet, S. Franchoo, A. Gadea, G. Georgiev, F. Ibrahim, B. Jacquot, T. Konstantinopoulos, S.M. Lenzi, G. Maquart, I. Matea, D. Mengoni, D.R. Napoli, T. Nikšić, L. Olivier, R.M. Pérez-Vidal, C. Portail, F. Recchia, N. Redon, M. Siciliano, I. Stefan, O. Stezowski, D. Vretenar, M. Zielinska, D. Barrientos, G. Benzoni, B. Birkenbach, A.J. Boston, H.C. Boston, B. Cederwall, L. Charles, M. Ciemala, J. Collado, D.M. Cullen, P. Désesquelles, G. de France, C. Domingo-Pardo, J. Eberth, V. González, L.J. Harkness-Brennan, H. Hess, D.S. Judson, A. Jungclaus, W. Korten, A. Lefevre, F. Legruel, R. Menegazzo, B. Million, J. Nyberg, B. Quintana, D. Ralet, P. Reiter, F. Saillant, E. Sanchis, C. Theisen, J.J. Valiente Dobon, Pseudospin symmetry and microscopic origin of shape coexistence in the ^{78}Ni region: a hint from lifetime measurements, Phys. Rev. Lett. 121 (2018) 192502. https://doi.org/10.1103/PhysRevLett.121.192502

[9] M. Madurga, R. Surman, I.N. Borzov, R. Grzywacz, K.P. Rykaczewski, C.J. Gross, D. Miller, D.W. Stracener, J.C. Batchelder, N.T. Brewer, L. Cartegni, J.H. Hamilton, J.K. Hwang, S.H. Liu, S.V. Ilyushkin, C. Jost, M. Karny, A. Korgul, W. Królas, A. Kuźniak, C. Mazzocchi, A.J. Mendez, K. Miernik, S.W. Padgett, S.V. Paulauskas, A.V. Ramayya, J.A. Winger, M. Woli ńska Cichocka, E.F. Zganjar, New half-lives of *r*-process Zn and Ga isotopes measured with electromagnetic separation, Phys. Rev. Lett. 109 (2012) 112501. https://doi.org/10.1103/PhysRevLett.109.112501

[10] A. Welker, N.A.S. Althubiti, D. Atanasov, K. Blaum, T.E. Cocolios, F. Herfurth, S. Kreim, D. Lunney, V. Manea, M. Mougeot, D. Neidherr, F. Nowacki, A. Poves, M. Rosenbusch, L. Schweikhard, F. Wienholtz, R.N. Wolf, K. Zuber, Binding energy of ^{79}Cu: probing the structure of the doubly magic ^{78}Ni from only one proton away, Phys. Rev. Lett. 119 (2017) 192502. https://doi.org/10.1103/PhysRevLett.119.192502

[11] L. Olivier, S. Franchoo, M. Niikura, Z. Vajta, D. Sohler, P. Doornenbal, A. Obertelli, Y. Tsunoda, T. Otsuka, G. Authelet, H. Baba, D. Calvet, F. Château, A. Corsi, A. Delbart, J.-M. Gheller, A. Gillibert, T. Isobe, V. Lapoux, M. Matsushita, S. Momiyama, T. Motobayashi, H. Otsu, C. Péron, A. Peyaud, E.C. Pollacco, J.-Y. Roussé, H. Sakurai, C. Santamaria, M. Sasano, Y. Shiga, S. Takeuchi, R. Taniuchi, T. Uesaka, H. Wang, K. Yoneda, F. Browne, L.X. Chung, Z. Dombradi, F. Flavigny, F. Giacoppo, A. Gottardo, K. Hadyńska-Klęk, Z. Korkulu, S. Koyama, Y. Kubota, J. Lee, M. Lettmann, C. Louchart, R. Lozeva, K. Matsui, T. Miyazaki, S. Nishimura, K. Ogata, S. Ota, Z. Patel, E. Sahin, C. Shand, P.-A. Söderström, I. Stefan, D. Steppenbeck, T. Sumikama, D. Suzuki, V. Werner, J. Wu, Z. Xu, Persistence of the $Z = 28$ shell gap around ^{78}Ni: first spectroscopy of ^{79}Cu, Phys. Rev. Lett. 119 (2017) 192501. https://doi.org/10.1103/PhysRevLett.119.192501

[12] R.P. de Groote, J. Billowes, C.L. Binnersley, M.L. Bissell, T.E. Cocolios, T. Day Goodacre, G.J. Farooq-Smith, D.V. Fedorov, K.T. Flanagan, S. Franchoo, R.F. Garcia Ruiz, A. Koszorús, K.M. Lynch, G. Neyens, F. Nowacki, T. Otsuka, S. Rothe, H.H. Stroke, Y. Tsunoda, A.R. Vernon, K.D.A. Wendt, S.G. Wilkins, Z.Y. Xu, X.F. Yang, Dipole and quadrupole moments of $^{73-78}$Cu as a test of the robustness of the $Z = 28$ shell closure near ^{78}Ni, Phys. Rev. C 96 (2017) 041302(R). https://doi.org/10.1103/PhysRevC.96.041302

[13] R. Orlandi, D. Mücher, R. Raabe, A. Jungclaus, S.D. Pain, V. Bildstein, R. Chapman, G. de Angelis, J.G. Johansen, P. Van Duppen, A.N. Andreyev, S. Bottoni, T.E. Cocolios, H. De Witte, J. Diriken, J. Elseviers, F. Flavigny, L.P. Gaffney, R. Gernhäuser, A. Gottardo, M. Huyse, A. Illana, J. Konki, T. Kröll, R. Krücken, J.F.W. Lane, V. Liberati, B. Marsh, K. Nowak, F. Nowacki, J. Pakarinen, E. Rapisarda, F. Recchia, P. Reiter, T. Roger, E. Sahin, M. Seidlitz, K. Sieja, J.F. Smith, J.J. Valiente Dobón, M. von Schmid, D. Voulot, N. Warr, F.K. Wenander, K. Wimmer, Single-neutron orbits near ^{78}Ni: spectroscopy of the $N = 49$ isotope ^{79}Zn, Phys. Lett. B 740 (2015) 298–302. https://doi.org/10.1016/j.physletb.2014.12.006

[14] Y. Shiga, K. Yoneda, D. Steppenbeck, N. Aoi, P. Doornenbal, J. Lee, H. Liu, M. Matsushita, S. Takeuchi, H. Wang, H. Baba, P. Bednarczyk, Z. Dombradi, Z. Fulop, S. Go, T. Hashimoto, M. Honma, E. Ideguchi, K. Ieki, K. Kobayashi, Y. Kondo, R. Minakata, T. Motobayashi, D. Nishimura, T. Otsuka, H. Otsu, H. Sakurai, N. Shimizu, D. Sohler, Y. Sun, A. Tamii, R. Tanaka, Z. Tian, Y. Tsunoda, Z. Vajta, T. Yamamoto, X. Yang, Z. Yang, Y. Ye, R. Yokoyama, J. Zenihiro, Investigating nuclear shell structure in the vicinity of ^{78}Ni: low-lying excited states in the neutron-rich isotopes ^{80,82}Zn, Phys. Rev. C 93 (2016) 024320. https://doi.org/10.1103/PhysRevC.93.024320

[15] C.M. Shand, Z. Podolyák, M. Górska, P. Doornenbal, A. Obertelli, F. Nowacki, T. Otsuka, K. Sieja, J.A. Tostevin, Y. Tsunoda, G. Authelet, H. Baba, D. Calvet, A. Château, S. Chen, A. Corsi, A. Delbart, J.M. Gheller, A. Giganon, A. Gillibert, T. Isobe, V. Lapoux, M. Matsushita, S. Momiyama, T. Motobayashi, M. Niikura, H. Otsu, N. Paul, C. Péron, A. Peyaud, E.C. Pollacco, J.-Y. Roussé, H. Sakurai, C. Santamaria, M. Sasano, Y. Shiga, D. Steppenbeck, S. Takeuchi, R. Taniuchi, T. Uesaka, H. Wang, K. Yoneda, T. Ando, T. Arici, A. Blazhev, F. Browne, A.M. Bruce, R.J. Carroll, L.X. Chung, M.L. Cortés, M. Dewald, B. Ding, Z. Dombrádi, F. Flavigny, S. Franchoo, F. Giacoppo, A. Gottardo, K. Hadyńska-Klęk, A. Jungclaus, Z. Korkulu, S. Koyama, Y. Kubota, J. Lee, M. Lettmann, B.D. Linh, J. Liu, Z. Liu, C. Lizarazo, C. Louchart, R. Lozeva, K. Matsui, T. Miyazaki, K. Moschner, M. Nagamine, N. Nakatsuka, S. Nishimura, C.R. Nita, C.R. Nobs, L. Olivier, S. Ota, R. Orlandi, Z. Patel, P.H. Regan, M. Rudigier, E. Şahin, T. Saito, P.-A. Söderström, I. Stefan, T. Sumikama, D. Suzuki, Z. Vajta, V. Vaquero, V. Werner, K. Wimmer, J. Wu, Z.Y. Xu, Shell evolution beyond $Z = 28$ and $N = 50$: spectroscopy of ^{81,82,83,84}Zn, Phys. Lett. B 773 (2017) 492–497. https://doi.org/10.1016/j.physletb.2017.09.001

[16] A. Gottardo, D. Verney, C. Delafosse, F. Ibrahim, B. Roussière, C. Sotty, S. Roccia, C. Andreoiu, C. Costache, M.-C. Delattre, I. Deloncle, A. Etilé, S. Franchoo, C. Gaulard, J. Guillot, M. Lebois, M. MacCormick, N. Marginean, R. Marginean, I. Matea, C. Mihai, I. Mitu, L. Olivier, C. Portail, L. Qi, L. Stan, D. Testov, J. Wilson, D.T. Yordanov, First evidence of shape coexistence in the ^{78}Ni region: intruder 0_2^+ state in ^{80}Ge, Phys. Rev. Lett. 116 (2016) 182501. https://doi.org/10.1103/PhysRevLett.116.182501

[17] L. Nies, L. Canete, D.D. Dao, S. Giraud, A. Kankainen, D. Lunney, F. Nowacki, B. Bastin, M. Stryjczyk, P. Ascher, K. Blaum, R.B. Cakirli, T. Eronen, P. Fischer, M. Flayol, V. Girard Alcindor, A. Herlert, A. Jokinen, A. Khanam, U. Köster, D. Lange, I.D. Moore, M. Müller, M. Mougeot, D.A. Nesterenko, H. Penttilä, C. Petrone, I. Pohjalainen, A. de Roubin, V. Rubchenya, C. Schweiger, L. Schweikhard, M. Vilen, J. Äystö, Further evidence for shape coexistence in ^{79}Zn^m near doubly magic ^{78}Ni, Phys. Rev. Lett. 131 (2023) 222503. https://doi.org/10.1103/PhysRevLett.131.222503

[18] Y. Shimizu, K.P. Rykaczewski, N. Fukuda, N.T. Brewer, I. Dillmann, R.K. Grzywacz, S. Nishimura, B.C. Rasco, J.L. Tain, H. Suzuki, H. Takeda, D.S. Ahn, T. Sumikama, N. Inabe, K. Yoshida, H. Ueno, S. Michimasa, A. Algora, J.M. Allmond, J. Agramunt, H. Baba, S. Bae, C.G. Bruno, R. Caballero-Folch, F. Calvino, P.J. Coleman-Smith, G. Cortes, T. Davinson, C. Domingo-Pardo, A. Estrade, S. Go, C.J. Griffin, J. Ha, O. Hall, L.J. Harkness-Brennan, J. Heideman, T. Isobe, D. Kahl, M. Karny, L.H. Khiem, T.T. King, G.G. Kiss, A. Korgul, S. Kubono, M. Labiche, I. Lazarus, J. Liang, J. Liu, G. Lorusso, M. Madurga, K. Matsui, K. Miernik, F. Montes, A.I. Morales, P. Morrall, N. Nepal, R.D. Page, V.H. Phong, M. Piersa-Siłkowska, M. Prydderch, V.F.E. Pucknell, M.M. Rajabali, B. Rubio, Y. Saito, H. Sakurai, J. Simpson, M. Singh, D.W. Stracener, A. Tarifeño-Saldivia, S.L. Thomas, A. Tolosa-Delgado, M. Wolinska-Cichocka, P.J. Woods, X.X. Xu, R. Yokoyama, Exploration of neutron-rich isotopes around $N = 50$ via the in-flight fission of a 345 MeV/nucleon ^{238}U beam, Prog. Theor. Exp. Phys. 2026 (3) (2026) 033D06. https://doi.org/10.1093/ptep/ptag036

[19] K. Sieja, F. Nowacki, Three-body forces and persistence of spin-orbit shell gaps in medium-mass nuclei: toward the doubly magic ^{78}Ni, Phys. Rev. C 85 (2012) 051301(R). https://doi.org/10.1103/PhysRevC.85.051301

[20] J.G. Li, Merging of the island of inversion at $N = 40$ and $N = 50$, Phys. Lett. B 840 (2023) 137893. https://doi.org/10.1016/j.physletb.2023.137893

[21] X.P. Wang, J.G. Li, N. Chen, Realistic shell model calculations for shell evolution near ^{78}Ni, Phys. Rev. C 111 (2025) 044308. https://doi.org/10.1103/PhysRevC.111.044308

[22] Y. Tsunoda, T. Otsuka, N. Shimizu, M. Honma, Y. Utsuno, Novel shape evolution in exotic Ni isotopes and configuration-dependent shell structure, Phys. Rev. C 89 (2014) 031301(R). https://doi.org/10.1103/PhysRevC.89.031301

[23] K. Yoshida, Suddenly shortened half-lives beyond ^{78}Ni : $N = 50$ magic number and high-energy nonunique first-forbidden transitions, Phys. Rev. C 100 (2019) 024316. https://doi.org/10.1103/PhysRevC.100.024316

[24] B.S. Hu, Z.H. Sun, G. Hagen, G.R. Jansen, T. Papenbrock, *Ab initio* computations from ^{78}Ni towards ^{70}Ca along neutron number $N = 50$, Phys. Lett. B 858 (2024) 139010. https://doi.org/10.1016/j.physletb.2024.139010

[25] A. Tichai, S. Knecht, A.T. Kruppa, Ö. Legeza, C.P. Moca, A. Schwenk, M.A. Werner, G. Zarand, Combining the in-medium similarity renormalization group with the density matrix renormalization group: shell structure and information entropy, Phys. Lett. B 845 (2023) 138139. https://doi.org/10.1016/j.physletb.2023.138139

[26] Z.C. Xu, R.Z. Hu, S.L. Jin, J.H. Hou, S. Zhang, F.R. Xu, Collectivity of nuclei near the exotic doubly magic ^{78}Ni by *ab initio* calculations, Phys. Rev. C 110 (2024) 024308. https://doi.org/10.1103/PhysRevC.110.024308

[27] A. Tichai, K. Kapás, T. Miyagi, M.A. Werner, Ö. Legeza, A. Schwenk, G. Zarand, Spectroscopy of $N = 50$ isotones with the valence-space density matrix renormalization group, Phys. Lett. B 855 (2024) 138841. https://doi.org/10.1016/j.physletb.2024.138841

[28] K. Tsukiyama, S.K. Bogner, A. Schwenk, In-medium similarity renormalization group for nuclei, Phys. Rev. Lett. 106 (2011) 222502. https://doi.org/10.1103/PhysRevLett.106.222502

[29] S.K. Bogner, H. Hergert, J.D. Holt, A. Schwenk, S. Binder, A. Calci, J. Langhammer, R. Roth, Nonperturbative shell-model interactions from the in-medium simi-

larity renormalization group, Phys. Rev. Lett. 113 (2014) 142501. https://doi.org/10.1103/PhysRevLett.113.142501
[30] T.D. Morris, N.M. Parzuchowski, S.K. Bogner, Magnus expansion and in-medium similarity renormalization group, Phys. Rev. C 92 (2015) 034331. https://doi.org/10.1103/PhysRevC.92.034331
[31] S.R. Stroberg, A. Calci, H. Hergert, J.D. Holt, S.K. Bogner, R. Roth, A. Schwenk, Nucleus-dependent valence-space approach to nuclear structure, Phys. Rev. Lett. 118 (2017) 032502. https://doi.org/10.1103/PhysRevLett.118.032502
[32] H. Hergert, S.K. Bogner, T.D. Morris, A. Schwenk, K. Tsukiyama, The in-medium similarity renormalization group: a novel *ab initio* method for nuclei, Phys. Rep. 621 (2016) 165–222. Memorial Volume in Honor of Gerald E. Brown. https://doi.org/10.1016/j.physrep.2015.12.007
[33] S.R. Stroberg, H. Hergert, S.K. Bogner, J.D. Holt, Nonempirical interactions for the nuclear shell model: an update, Annu. Rev. Nucl. Part. Sci. 69 (2019) 307–362. https://doi.org/10.1146/annurev-nucl-101917-021120
[34] C. Stumpf, J. Braun, R. Roth, Importance-truncated large-scale shell model, Phys. Rev. C 93 (2016) 021301(R). https://doi.org/10.1103/PhysRevC.93.021301
[35] R. Roth, Importance truncation for large-scale configuration interaction approaches, Phys. Rev. C 79 (2009) 064324. https://doi.org/10.1103/PhysRevC.79.064324
[36] A.A. Holmes, N.M. Tubman, C.J. Umrigar, Heat-bath configuration interaction: an efficient selected configuration interaction algorithm inspired by heat-bath sampling, J. Chem. Theory Comput. 12 (8) (2016) 3674–3680. PMID: 27428771. https://doi.org/10.1021/acs.jctc.6b00407
[37] S. Sharma, A.A. Holmes, G. Jeanmairet, A. Alavi, C.J. Umrigar, Semistochastic heat-bath configuration interaction method: selected configuration interaction with semistochastic perturbation theory, J. Chem. Theory Comput. 13 (4) (2017) 1595–1604. PMID: 28263594. https://doi.org/10.1021/acs.jctc.6b01028
[38] J. Li, M. Otten, A.A. Holmes, S. Sharma, C.J. Umrigar, Fast semistochastic heat-bath configuration interaction, J. Chem. Phys. 149 (21) (2018) 214110. https://doi.org/10.1063/1.5055390
[39] A.A. Holmes, C.J. Umrigar, S. Sharma, Excited states using semistochastic heat-bath configuration interaction, J. Chem. Phys. 147 (16) (2017) 164111. https://doi.org/10.1063/1.4998614
[40] D.R. Entem, R. Machleidt, Accurate charge-dependent nucleon-nucleon potential at fourth order of chiral perturbation theory, Phys. Rev. C 68 (2003) 041001(R). https://doi.org/10.1103/PhysRevC.68.041001
[41] K. Hebeler, S.K. Bogner, R.J. Furnstahl, A. Nogga, A. Schwenk, Improved nuclear matter calculations from chiral low-momentum interactions, Phys. Rev. C 83 (2011) 031301(R). https://doi.org/10.1103/PhysRevC.83.031301
[42] J. Simonis, S.R. Stroberg, K. Hebeler, J.D. Holt, A. Schwenk, Saturation with chiral interactions and consequences for finite nuclei, Phys. Rev. C 96 (2017) 014303. https://doi.org/10.1103/PhysRevC.96.014303
[43] S.R. Stroberg, IMSRG++: in-medium similarity renormalization group software for nuclear structure calculations, https://github.com/ragnarstroberg/imsrg.
[44] T. Miyagi, A numerical code to generate nuclear two- and three-body matrix elements from chiral effective field theory, Eur. Phys. J. A 59 (2023) 150. https://doi.org/10.1140/epja/s10050-023-01039-y
[45] R. Roth, P. Navrátil, Ab initio study of ^{40}Ca with an importance-truncated no-core shell model, Phys. Rev. Lett. 99 (2007) 092501. https://doi.org/10.1103/PhysRevLett.99.092501
[46] M.K.G. Kruse, E.D. Jurgenson, P. Navrátil, B.R. Barrett, W.E. Ormand, Extrapolation uncertainties in the importance-truncated no-core shell model, Phys. Rev. C 87 (2013) 044301. https://doi.org/10.1103/PhysRevC.87.044301
[47] R. Roth, J. Langhammer, A. Calci, S. Binder, P. Navrátil, Similarity-transformed chiral $NN+3N$ interactions for the ab initio description of ^{12}**C** and ^{16}**O**, Phys. Rev. Lett. 107 (2011) 072501. https://doi.org/10.1103/PhysRevLett.107.072501
[48] R. Roth, A. Calci, J. Langhammer, S. Binder, Evolved chiral $NN+3N$ Hamiltonians for ab initio nuclear structure calculations, Phys. Rev. C 90 (2014) 024325. https://doi.org/10.1103/PhysRevC.90.024325
[49] https://www.nndc.bnl.gov/ensdf/.
[50] M.-G. Porquet, O. Sorlin, Evolution of the $N=50$ gap from $Z=30$ to $Z=38$ and extrapolation toward ^{78}Ni, Phys. Rev. C 85 (2012) 014307. https://doi.org/10.1103/PhysRevC.85.014307
[51] M. Wang, W.J. Huang, F.G. Kondev, G. Audi, S. Naimi, The AME 2020 atomic mass evaluation (II). Tables, graphs and references*, Chin. Phys. C 45 (3) (2021) 030003. https://doi.org/10.1088/1674-1137/abddaf
[52] T. Ohnishi, T. Kubo, K. Kusaka, A. Yoshida, K. Yoshida, M. Ohtake, N. Fukuda, H. Takeda, D. Kameda, K. Tanaka, N. Inabe, Y. Yanagisawa, Y. Gono, H. Watanabe, H. Otsu, H. Baba, T. Ichihara, Y. Yamaguchi, M. Takechi, S. Nishimura, H. Ueno, A. Yoshimi, H. Sakurai, T. Motobayashi, T. Nakao, Y. Mizoi, M. Matsushita, K. Ieki, N. Kobayashi, K. Tanaka, Y. Kawada, N. Tanaka, S. Deguchi, Y. Satou, Y. Kondo, T. Nakamura, K. Yoshinaga, C. Ishii, H. Yoshii, Y. Miyashita, N. Uematsu, Y. Shiraki, T. Sumikama, J. Chiba, E. Ideguchi, A. Saito, T. Yamaguchi, I. Hachiuma, T. Suzuki, T. Moriguchi, A. Ozawa, T. Ohtsubo, M.A. Famiano, H. Geissel, A.S. Nettleton, O.B. Tarasov, D.P. Bazin, B.M. Sherrill, S.L. Manikonda, J.A. Nolen, Identification of 45 new neutron-rich isotopes produced by in-flight fission of a ^{238}U beam at 345 MeV/nucleon, J. Phys. Soc. Jpn. 79 (7) (2010) 073201. https://doi.org/10.1143/JPSJ.79.073201
[53] A. Jacobs, S. Nikas, J. Ash, B. Ashrafkhani, I. Belosovic, J. Bergmann, C. Brown, J. Cardona, E. Dunling, T. Dickel, L. Egoriti, G. Gelinas, Z. Hockenbery, S. Kakkar, B. Kootte, A. Mollaebrahimi, E.M. Lykiardopoulou, T. Murböck, S. Paul, W.R. Plaß, W.S. Porter, M.P. Reiter, A. Ridley, J. Ringuette, C. Scheidenberger, R. Simpson, C. Walls, Y. Wang, J. Dilling, A. Kwiatkowski, Direct mass measurements of neutron-rich zinc and gallium isotopes: an investigation of the formation of the first *r*-process peak, Phys. Rev. Lett. 134 (2025) 062701. https://doi.org/10.1103/PhysRevLett.134.062701
[54] M.V. Stoitsov, J. Dobaczewski, W. Nazarewicz, S. Pittel, D.J. Dean, Systematic study of deformed nuclei at the drip lines and beyond, Phys. Rev. C 68 (2003) 054312. https://doi.org/10.1103/PhysRevC.68.054312
[55] V.N. Tarasov, D.V. Tarasov, K.A. Gridnev, D.K. Gridnev, V.G. Kartavenko, W. Greiner, J. Hamilton, V.I. Kuprikov, Properties of Fe, Ni and Zn isotope chains near the drip-line, in: Fission and Properties of Neutron-Rich Nuclei, 2008, pp. 697–699. https://doi.org/10.1142/9789812833433_0088
[56] P. Möller, A.J. Sierk, T. Ichikawa, H. Sagawa, Nuclear ground-state masses and deformations: FRDM(2012), At. Data Nucl. Data Tables 109-110 (2016) 1–204. https://doi.org/10.1016/j.adt.2015.10.002